Influence of Axisymmetric Assumptions on Large Eddy Simulations of a Confined Jet and a Swirl Flow

Jörg Schlüter*

CERFACS
42, Av. Gaspard Coriolis
31057 Toulouse Cedex 1
France

October 22, 2001

Abstract

Many practical flow problems are situated in axisymmetric geometries. RANS flow solvers can lower the computational efforts dramatically by taking this axisymmetry into account and computing only a segment of the flow. However, the extension of this concept to LES computations is not straight forward, since the boundary conditions imposed on the axis of symmetry are altering the instantaneous flow field. In this study, the importance of the introduction of an axis of symmetry to LES computations is assessed by computations of a flow with and without swirl over an axisymmetric expansion. The LES computations are performed on a full 3D mesh and a 90° segment of the geometry. The results are compared and the influence of the axis is put into relation with the gain in computational costs.

1 Introduction

Numerical tools based on the Reynolds-averaged Navier-Stokes (RANS) formulation have entered the industrial engineering cycle since many years. They offer especially in the field of combustion research and gas turbine combustors crucial informations which can not be gathered by experimental investigations [Krebs et al., 1999].

*current address: Stanford University, Center for Turbulence Research, Bldg. 500, Stanford, CA, 94305-3030, USA, Jorg.Schluter@stanford.edu

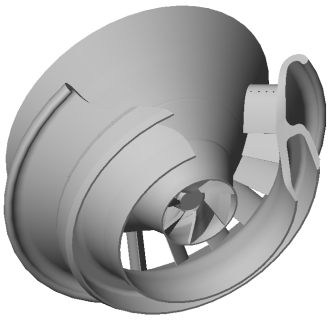

Figure 1: Deviation model of a gas turbine burner

In the recent time, the advantages of Large Eddy Simulations (LES) have been noticed by industry. In the area of combustion research, the resolution of the time-developing flow field delivers a variety of additional information which can be used for the modeling of flames [Pierce and Moin, 1998a], [Colin et al., 2000]. However, the huge computational costs of LES are still a hurdle for industry to accept LES as an everyday tool. Worldwide efforts are made to optimize flow solvers and models in order to to render LES as attractive as RANS for industrial applications.

Many practical flow problems are situated in axisymmetric geometries. One possibility of RANS flow solvers to lower computational efforts in these cases is to take the axisymmetry of the geometry and the Reynolds-averaged flow field into account and to compute only a pie-segment of the flow. As an example can be taken the swirl flow of an industrial gas turbine burner (Fig. 1). The complex geometry with a multitude of vanes and injection systems lets the number of mesh points climb easily to over twelve million mesh points, even if a very coarse mesh is applied [Schlüter, 2000]. In an industrial framework, an LES computation would be not feasible, if a considerable long physical time-span is to be computed. In this particular case, with the assumption of axisymmetry the geometry can be cut down to a 20° angle of the burner and the number of mesh points reduced by a factor of 18.

However, the extension of this concept of axisymmetry to LES computations meets some problems. While the geometry and the time-averaged quantities may be axisymmetric, the instantaneous flow field is not. Thus, the boundary conditions which have to be imposed on the axis of symmetry will alter the flow field and introduce an error. This additional error might not be an obstacle for industrial applications, if it is small enough to justify this approach in order to keep computational costs low. Aim of the present LES investigation is to quantify the effect of the axisymmetric approach to LES computations, particularly with regard to LES of swirl flows. In order to assess the importance of the error and to determine the gain of computational resources, the investigation reported here performs LES computations on two different flows and each on two different mesh geometries.

2 Problem Setup

2.1 Swirl Flows

Since swirl flows can be found in numerous industrial applications like cyclone separators, flow over delta wings and especially swirl combustors, many experimental investigations dealt with the investigation of swirl flows (e.g. [Faler and Leibovich, 1977], [Faler and Leibovich, 1978], [Escudier and Zehnder, 1982], [Farokhi et al., 1989] and many others). However, since swirl flows are sensitive to exterior influences [Gupta et al., 1984] the numerical investigation of swirl flows is difficult.

RANS flow solvers are able to reproduce the basic flow features of the vortex breakdown [Hogg and Leschziner, 1989] and even dynamic features like precessing vortex cores [Guo et al., 2001]. However, the comparison of the numerical results against experimental data is not always satisfactory.

The highly unsteady nature of swirl flows makes numerical flow solvers based on an LES formulations more promising. Several investigations have shown, that LES computations are able to compute the jet [Akselvoll and Moin, 1996] and swirl [Pierce and Moin, 1998a] characteristics of a typical swirl combustor geometry and are able to reproduce experimental investigations accurately. The drawback of these computations were a high spatial discretization of the problem and, as a consequence thereof, high computational costs.

The current investigation tries to evaluate possibilities to reduce the computational costs of LES of swirl flows.

2.2 Flow Configurations

The present LES computations try to reproduce the results from the experimental investigation of Dellenback [Dellenback, 1986], [Dellenback et al., 1988] on a flow at an an abrupt axisymmetric expansion (Fig. 2). This experimental investigation has well documented flow parameters and velocity profiles taken by LDA measurements upstream and downstream of the expansion. This gives a clear definition of the inlet boundary conditions and the possibility to compare the flow development closely. The expansion ratio is about 1:2 which leads to a cross section area ratio of 1:4. This geometry and flow configuration can be seen as an idealized gas turbine combustor.

In the experimental investigation the flow with different swirl numbers S,

$$S = \frac{1}{R} \frac{\int_0^\infty r^2 \bar{u}\bar{w} dr}{\int_0^\infty r\bar{u}^2 dr} \tag{1}$$

were investigated.

The LES computations will concentrate on two flow configurations:

1. The flow without swirl (S=0.0). Here, a simple axisymmetric step flow is examined.

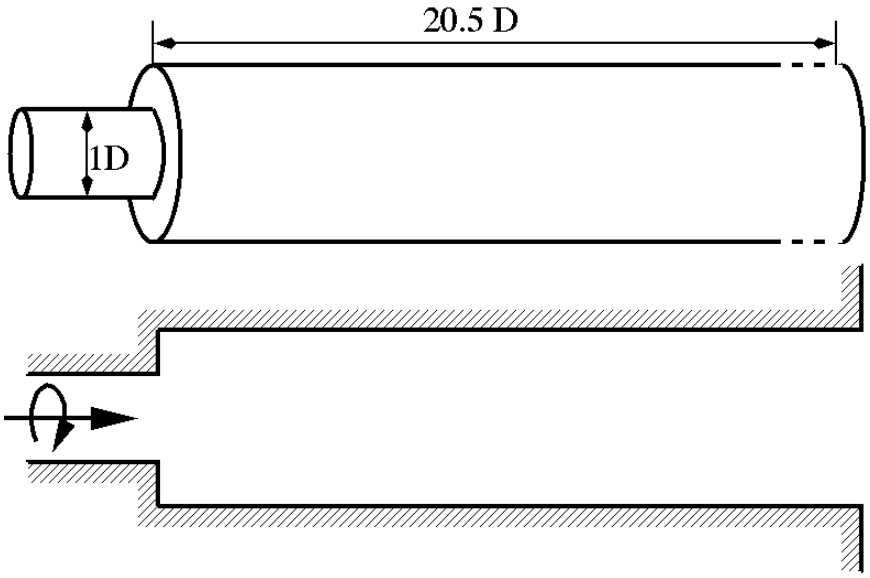

Figure 2: geometry of the test-case

2. The flow with a strong swirl (S=0.6). Here, vortex breakdown takes place and the effect of the axis of symmetry on the recirculation zone can be investigated.

Both flow configurations are computed at a Reynolds-number Re=30,000.

2.3 Mesh Geometries

The computations are performed on two different meshes (Fig. 3):

1. A full three-dimensional mesh, which is the usual way to perform an LES computation.

2. A 90° pie segment of the axisymmetric geometry.

Furthermore, a so called 2D axisymmetric mesh has been used created by a very thin slice of the axisymmetric geometry and only one cell in azimuthal direction. Although the 2D computation can not be seen as a real LES computation, since the turbulence in the third direction is strongly disturbed, 2D LES and DNS computations have shown some potential in cases, where not the turbulence itself was subject of research, but chemical processes or model development. However, the computational results of the 2D computations had very strong disagreements, quantitatively as well as qualitatively, so that this approach has been abandoned. This underlines the fact, that turbulence has always to be treated as a three dimensional phenomenon.

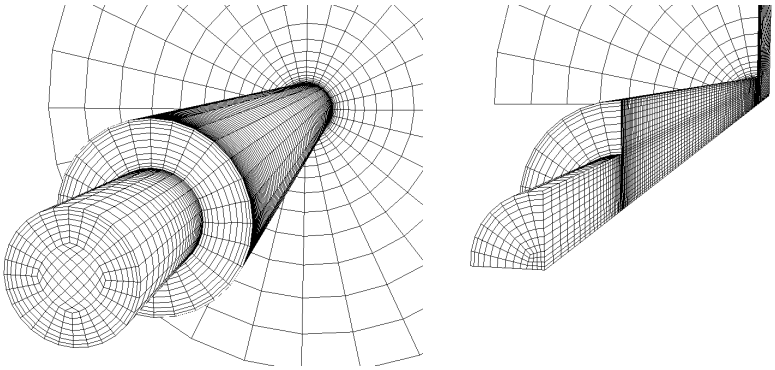

Figure 3: Meshes used for the swirl flow investigation. full 3D geometry (left), 90° axi-symmetric cut (center) and 2D axi-symmetric mesh (right)

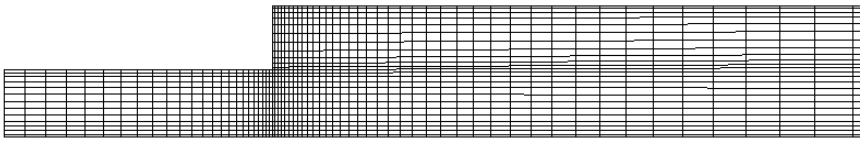

Figure 4: Side view on the 90° axi-symmetric mesh near the step, the axis of symmetry is below

Care was taken to generate both meshes so that they resemble each other as best as possible, although it was necessary to modify them close to the axis. The meshes are structured meshes. The computational domain starts two diameter D upstream of the step. The test section is $20.5D$ long and ends in a chamber with a diameter of $20D$ (Fig. 4). The chamber downstream of the test-section is part of the computed domain and ends $10D$ downstream in a non-reflecting outlet. On the surfaces of the walls lies an O-grid. The thickness of the first cell on the surface has a $y^+ = 35$. This mesh is around $\frac{1}{4}D$ thick.

The full 3D mesh has an H-mesh in the center and consists in total of 75000 mesh points.The 90° axi-symmetric mesh has also an H-mesh in the center, albeit shifted, so that one edge of the H-mesh forms the axis of symmetry. This mesh has a size of 22000 points.

An additional finer full 3D mesh with 410,000 mesh points and a $y^+ = 15$ was created in order to assess the sensitivity of LES to the mesh size.

2.4 Inlet Conditions

It seems favorable to start with the computations well upstream in order to not disturb the vortex roll-up at the step by a closely spaced domain inlet. Fortunately, in the experimental investigation flow measurements were made two diameters upstream of the step. This gives the possibility to let the computa-

tions start at this point.

The measurements indicate, that there is already turbulence present at this location. The possibilities to impose fully developed turbulence at the inlet of a domain is limited in LES, since temporally evolving boundary conditions have to be imposed. This can be done by a computation of a turbulent pipe flow in the preprocessing process and by using the data from this computation as boundary conditions [Pierce and Moin, 1998b]. However, it is difficult to define these boundary conditions on both mesh geometries likewise. In order to ensure that differences between the computations on the two meshes are solely effects from the axisymmetric approach and not from the boundary conditions, laminar velocity profiles in shape of the measured profiles are imposed at the inlet.

2.5 Axisymmetric Approach

The impact of the assumption of axisymmetry for the flow can be described as followed. In an axi-symmetric coordinate system ($[x, r, \phi]$ with the velocity components $[u_x, u_r, u_\phi]$ respectively) the following boundary conditions have to be applied on the axis: $u_r = 0$, $u_\phi = 0$ and $\frac{\partial u_x}{\partial r} = 0$.

In a Reynolds-averaged approach this can be fulfilled easily under the assumption of symmetric temporal mean values. For an unsteady approach however, like LES, these boundary conditions have to be applied at *every instant*. Although the geometry might be axi-symmetric, the turbulence is not. Since it is assumed, that u_r and u_ϕ are zero on the axis, these quantities have a turbulence intensity of zero at the axis as well. In the case of u_r it means, that there is no turbulent transport crosswise from the axis. Furthermore it has to be mentioned, that many unsteady non-axisymmetric flow instabilities exist. The phenomenon of so called *precessing vortex cores* is the most common non-axisymmetric flow instability in swirl flows [Gupta et al., 1984]. It has been shown, that LES of the full 3D geometry is a very powerful tool to investigate these instabilities [Schlüter et al., 2001]. Of course, an axisymmetric approach is unsuitable to address this particular problem, which might introduce another error.

3 The Flow Solver

3.1 Mathematical Formulation

The basic idea of LES is to resolve the larger scales of motion of the turbulence while approximating the smaller ones. To achieve this, a filter is applied to the continuity equation and the transport equations of momentum. Applying the Favre filter

$$\overline{\rho}\widetilde{Q} = \overline{\rho Q} = \int_{-\infty}^{+\infty} \rho Q\,(x,t)\,G\,(x - x')\,dx' \tag{2}$$

leads to the following equations for momentum u_i:

$$\frac{\partial \bar{\rho}\widetilde{u_i}}{\partial t} + \frac{\partial \bar{\rho}\widetilde{u_i}\widetilde{u_j}}{\partial x} + \frac{\partial \overline{p}}{\partial x} = \frac{\overline{\partial \tau_{ij}}}{\partial x_j} + \frac{\partial T_{ij}}{\partial x_j} \quad \text{with } (i,j=1,2,3) \tag{3}$$

3.2 Subgrid Scale Model

The term T_{ij} results from the convective terms $\widetilde{u_i}\widetilde{u_j}$, which is split into a resolved part on the left hand side of the equation directly delivered by the LES calculation and an unresolved part on the right hand side, which needs to be modeled.

An eddy viscosity approach is used for the subgrid scales:

$$T_{ij} = 2\nu_t \overline{S}_{ij} + \frac{1}{3} T_{ll} \delta_{ij} \tag{4}$$

with

$$\overline{S}_{ij} = \frac{1}{2}\left(\frac{\partial u_i}{\partial x_j} + \frac{\partial u_j}{\partial x_i}\right) \tag{5}$$

The simplicity of this model allows fast computations and hence a higher spatial discretization and an increase of the resolved part of the spectrum.

To determine the eddy viscosity ν_t the Filtered Smagorinsky model [Ducros et al., 1997] defined on a high-pass filter HP was used:

$$\nu_t = (C_2 \Delta x)^2 \sqrt{2HP(\tilde{S}_{ij})HP(\tilde{S}_{ij})} \text{ with } C_2 = 0.37 \tag{6}$$

The high pass filter HP filters out the lower half of the resolved frequency including the mean flow (0Hz). This means, the eddy viscosity is only active on velocity gradients due to high frequent fluctuations. Thus, it is zero at the wall and in laminar flows. This model offers an improved behavior in transitional flows than the Standard Smagorinsky model [Smagorinsky, 1963] and was optimized to work for wall boundary layers.

3.3 Present Implementation

For the LES calculations the AVBP parallel solver developed at CERFACS and the Oxford University [Schönfeld and Rudgyard, 1999], based on the parallel library COUPL [Schönfeld and Rudgyard, 1998] was used. The program handles structured and unstructured meshes and is second-order accurate in space and and third order accurate in time. It is based on a compressible formulation of the Navier-Stokes equations. The Navier-Stokes characteristic boundary conditions (NSCBC) have been implemented [Poinsot and Lele, 1992].

Although other flow solvers might have been more efficient for this particular problem (incompressible, structured), it was also aim to proof, that this flow solver is able to compute swirl flows in order to extend the investigation to reacting flows in complex gas turbine burners.

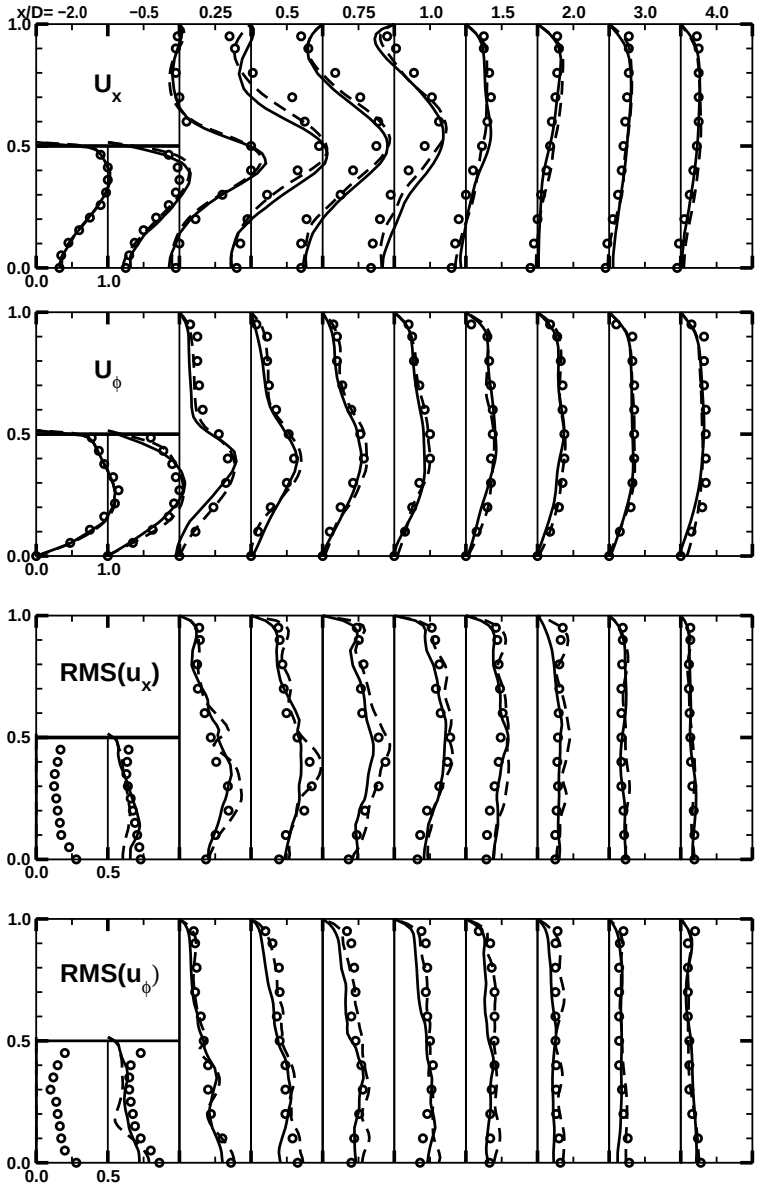

Figure 5: Influence of mesh coarsening. Profiles for swirl number S=0.6 (strong swirl). circles: measurements, solid line: LES on mesh with 75,000 points, dashed line: LES on mesh with 410,000 points. Averaging time-span 0.1s

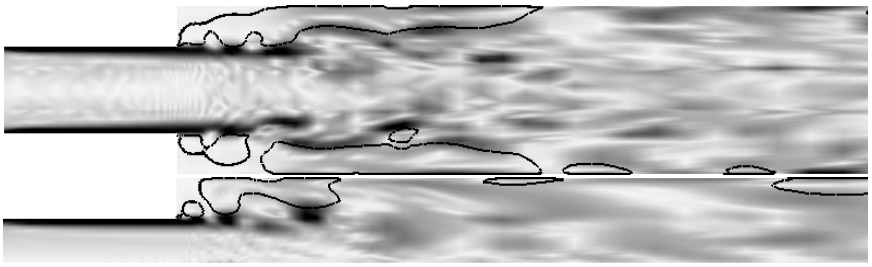

Figure 6: S=0.0, magnitude of azimuthal vorticity component of an instantaneous snapshot of the flow field (black: maximum, white: minimum), black line indicates recirculation zone, above: 3D full, below: 3D 90° axi-symmetric.

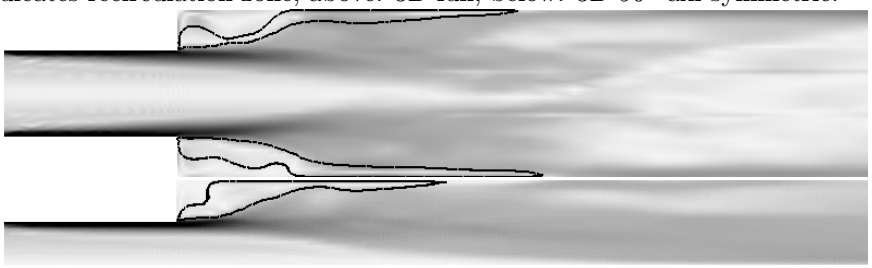

Figure 7: S=0.0, magnitude of azimuthal vorticity component of the time-averaged flow field (black: maximum, white: minimum), black line indicates recirculation zone, above: 3D full, below: 3D 90° axi-symmetric, averaging time-span: 0.2s

4 Computational Results

4.1 Accuracy of Mesh Resolution

Since long averaging time-spans are considered crucial to obtain proper statistical data, it is desirable to use coarse meshes in order to speed-up the computations and to compute long physical time-spans. In order to determine the influence of mesh coarsening one exemplary computation was performed on two different meshes, one on a coarse mesh with 75,000 mesh points, and the other a fine mesh with 410,000 mesh points.

To compute the same physical time-span, the computation on the coarse mesh was about nine times faster than on the fine mesh. This can be associated to two effects. First, the computation of less mesh points takes obviously less time. Second, on the coarse mesh larger time-step between two iterations can be used, since an acoustic wave needs more time to propagate between two adjacent mesh points.

Fig. 5 depicts the velocity profiles obtained by the computations and compares them to measurements for the case with a swirl number S=0.6. It can be seen, that both computations are in good agreement with the experiment.

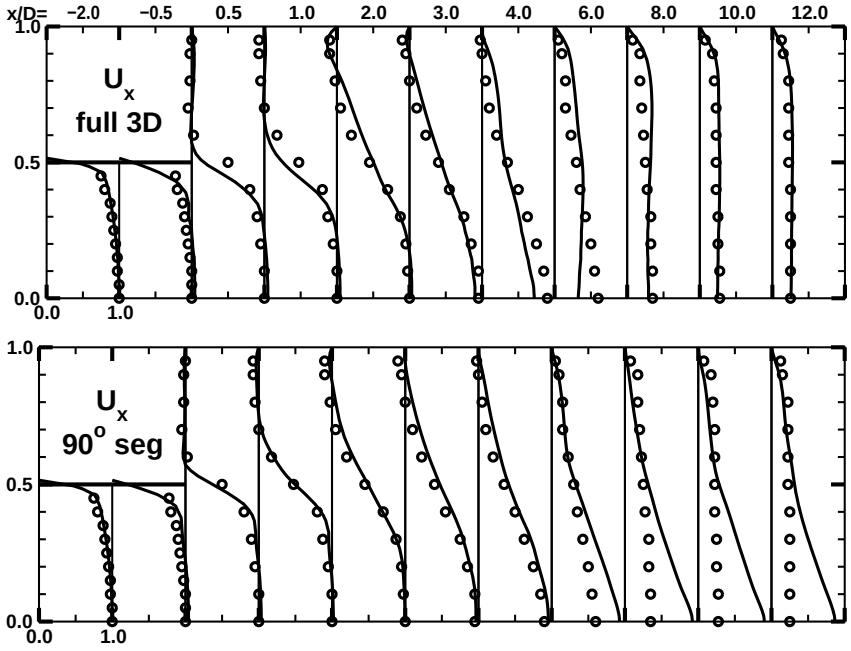

Figure 8: Expansion flow, S=0.0 (no swirl), $\overline{u}_x$ axial component, solid lines: LES computation, circles: experimental data, above: 3D full, below: 3D 90° axi-symmetric, averaging time-span: 0.2s

The computation on the fine mesh is in a slightly better agreement than the computation on a coarse mesh. Nevertheless, the improvement of the results by the refinement of the mesh do not justify the increased computational costs. The coarse mesh does predict reasonably well the swirl flow.

4.2 Axisymmetric Approach: No Swirl S=0.0

The investigation of the influence of the axisymmetric approach has been done on the coarser mesh. First, the case without any swirl (S=0.0) is examined. Fig. 6 depicts an instantaneous snapshot of the vorticity distribution of this case. In both computations the roll-up of coherent structures at the step can be seen. About 4 to 5 diameter downstream of the step the coherent structures are destroyed and only small scale structures exist.

While the initial vortex roll-up in the full 3D case appears to be nearly axisymmetric, further downstream the axisymmetry is lost and some vortex structures even cross the axis. The time averaged vorticity field of these two computations is illustrated in fig. 7. The recirculation zones, indicated by a black line, demonstrate deviations in the shape. Since the recirculation zones in the full 3D computation exhibit deviations on the upper and the lower part of the

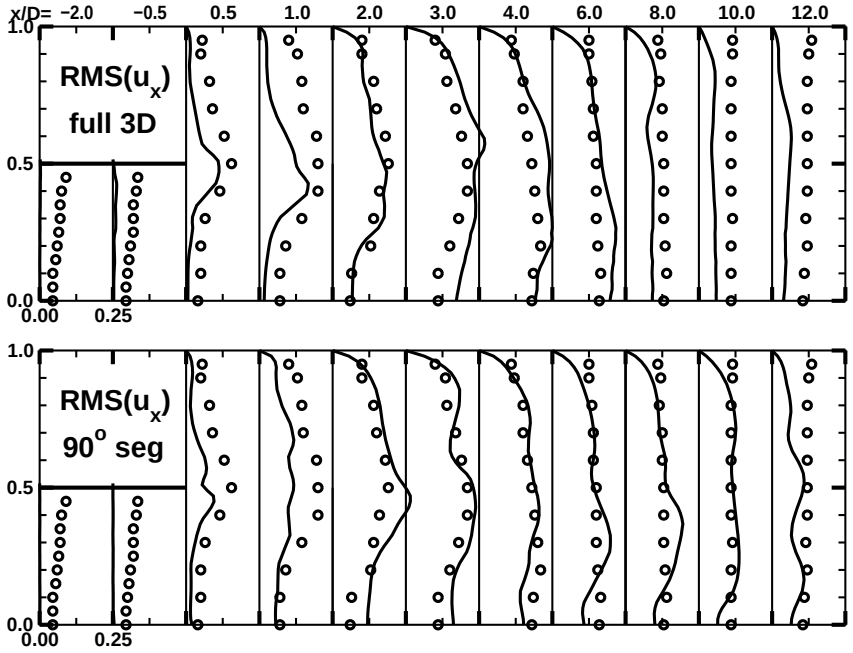

Figure 9: Expansion flow, S=0.0 (no swirl), $\overline{u_x'^2}$ axial turbulence intensity, solid lines: LES computation, circles: experimental data, above: 3D full, below: 3D 90° axi-symmetric, averaging time-span: 0.2s

step, the divergence of the full 3D and the 3D 90° axi-symmetric computation can be explained by the fact, that the averaging time span was not sufficiently long.

Fig. 8 depicts a comparison between the computations and the measurements of the time-averaged axial velocity $\overline{u}_x$. The outermost left profile is the profile which was imposed at the inlet, which explains the overall accordance in this profile. The second profile from the left was taken still upstream of the step. All other profiles are taken at different downstream positions behind the step.

In the case, where the full geometry was computed, the computation of the expansion flow is in good agreement with the measurements in the axial velocity component. There are slight differences in the spreading rate of the mixing layer close to the step. The reattachment length is well determined. Various former computations, especially RANS computations, had difficulties to determine this length properly [Rodi, 1996].

The 3D 90° axi-symmetric computation has greater deviations, especially close to the axis. While the reattachment length is well determined, there is a surplus of axial momentum close to the axis. This surplus can be assigned to the problem, that there is no turbulent radial component $\overline{u_r'^2}$ on the axis. Hence,

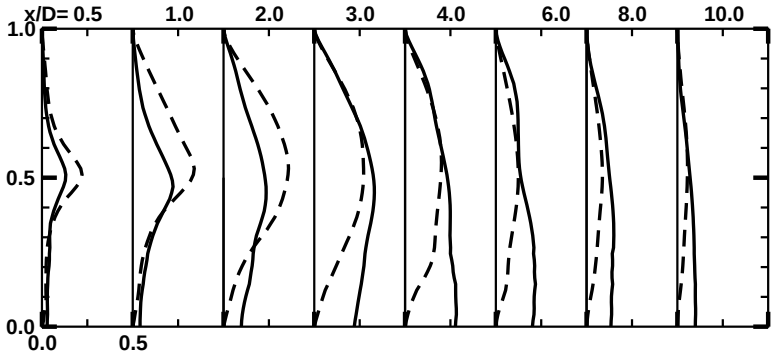

Figure 10: Expansion flow, S=0.0 (no swirl), $\overline{u_r'^2}$ radial turbulence intensity, solid lines: full 3D LES, dashed lines: 90° segment LES, averaging time-span: 0.2s

there is no *turbulent* transport from the axis to the outer flow. Initially, in the upstream pipe, the velocity maximum is located on the axis. This momentum can be transported to the rest of the flow only by *viscous* transport.

In the experimental investigation the axial turbulent intensity $\overline{u_x'^2}$ (fig. 9) was measured. Comparing the experimental data to the full 3D LES computation, it can be stated, that the turbulent axial velocities are underestimated. This is probably due to the fact, that the inlet of the computed domain is too close to the step and the turbulence is not fully developed in the upstream pipe.

In order to clarify the problem of the description of the radial turbulence component $\overline{u_r'^2}$, fig. 10 depicts the development of this quantity behind the step. Unfortunately no measured data is available, but since the full 3D LES computation has a good agreement with the experiment, the full 3D LES case can be taken as a reference of what to expect in an experiment. Directly behind the step, the turbulence is concentrated near the mixing layer of the jet and even in the full 3D case no turbulence has yet arrived near the axis. This is the reason, why the agreement between the full 3D and the 90° segment computations is still high (fig. 8) at this point. Further downstream in the full 3D case the maximum of the turbulence intensity of the radial velocity component shifts towards the centerline of the geometry. Since the axial symmetric computation does not predict any turbulence in radial direction on the axis the profiles start to disagree with the full 3D case, and the profiles of the axial velocity begin to disagree near the axis (fig. 8).

4.3 Axisymmetric Approach: Strong Swirl S=0.6

Adding swirl upstream of the expansion alters the flow field dramatically. Fig. 11 shows an instantaneous snapshot of the vorticity distribution and the recirculation zone. At this swirl number, vortex breakdown takes place and a recirculation zone on the axis develops. In the full 3D computation this recir-

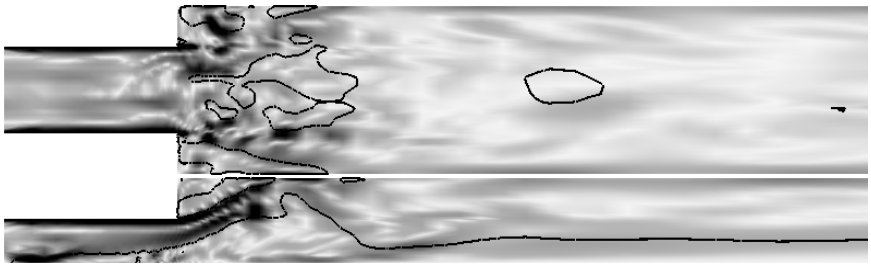

Figure 11: S=0.6, magnitude of azimuthal vorticity component of an instantaneous snapshot of the flow field (black: maximum, white: minimum), black line indicates recirculation zone, above: 3D full, below: 3D 90° axi-symmetric

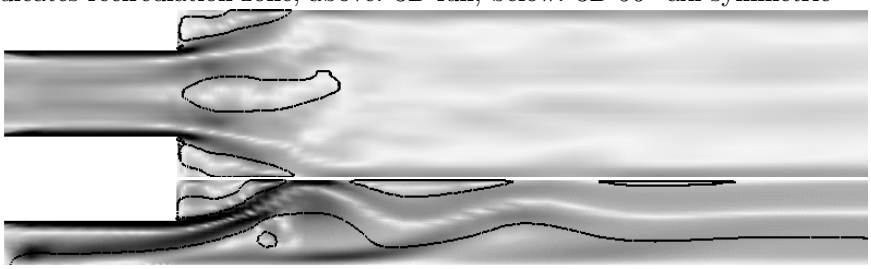

Figure 12: S=0.6, magnitude of azimuthal vorticity component of the time-averaged flow field (black: maximum, white: minimum), black line indicates recirculation zone, above: 3D full, below: 3D 90° axi-symmetric, averaging time-span: 0.2s

culation zone starts near the expansion and closes 1.5 diameter downstream. It is highly distorted by turbulence and is not axi-symmetric.

The shape of the recirculation zone in the axi symmetric computation is remarkably different to the recirculation zone in the full 3D computation. The recirculation zone crawls upstream close to the inlet of the domain and it does not close downstream.

Fig. 12 depicts the vorticity distribution of the time-averaged flow field. It can be seen, that the axi-symmetric computation disagrees qualitatively with the full 3D case.

Fig 13 compares the axial velocities $\overline{u}_x$ of the LES computation with the experimental data. Both computations determine the reattachment of the flow at the outer wall well. The full 3D computation is in good agreement with the experiment, although the thickness of the recirculation zone is underestimated.

In the experiment, the recirculation zone does not close downstream, while the full 3D LES computation predicts a weak positive axial velocity on the axis far behind the step. It has to be mentioned, that in the unsteady flow field, some pockets of the recirculating zone are floating downstream from time to time. In fig. 11 a detached recirculating zone floating downstream can be seen in the full 3D computation. It is probable, that the recirculation on the axis in the far

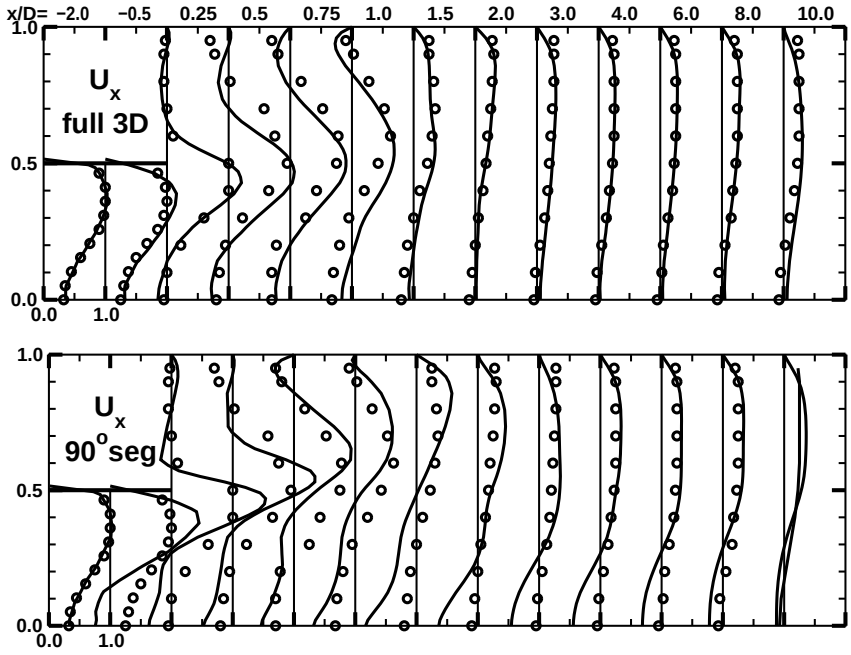

Figure 13: Expansion flow, S=0.6, $\overline{u}_x$ axial component, solid lines: LES computation, circles: experimental data, above: 3D full, below: 3D 90° axi-symmetric, averaging time-span: 0.2s

field of the experiment is a product of a frequent passing of these recirculation bubbles and that the LES computation underestimates the frequency of the detachments of recirculating bubbles.

An unsteady approach to examine the recirculation zone is mandatory for the following reason: looking on the experimental Reynolds-averaged flow field, the impression of a connected weak recirculation zone from the expansion to the outlet far downstream is given. Looking at the LES computation, frequent bubbles of strong recirculation zones passing the test section can be found. In the first case, fluid mass from far downstream is convected upstream to the expansion, while this is not the case in the unsteady approach.

The axi-symmetric computation overestimates the strength of the inner recirculation zone. The overestimation of the momentum on the axis was already explained in the unswirled case. It is due to the lack of turbulent momentum exchange in radial direction. The turbulence in radial direction is probably one important factor for the frequent detachment of the recirculating bubbles.

For the full 3D case the agreement between LES and experiment of the axial turbulence intensity $\overline{u_x'^2}$ is better than in the unswirled case (fig. 14). Obviously, the turbulence created by the recirculation zone is much higher than the free-stream turbulence in the arriving pipe flow. This underlines the capability of

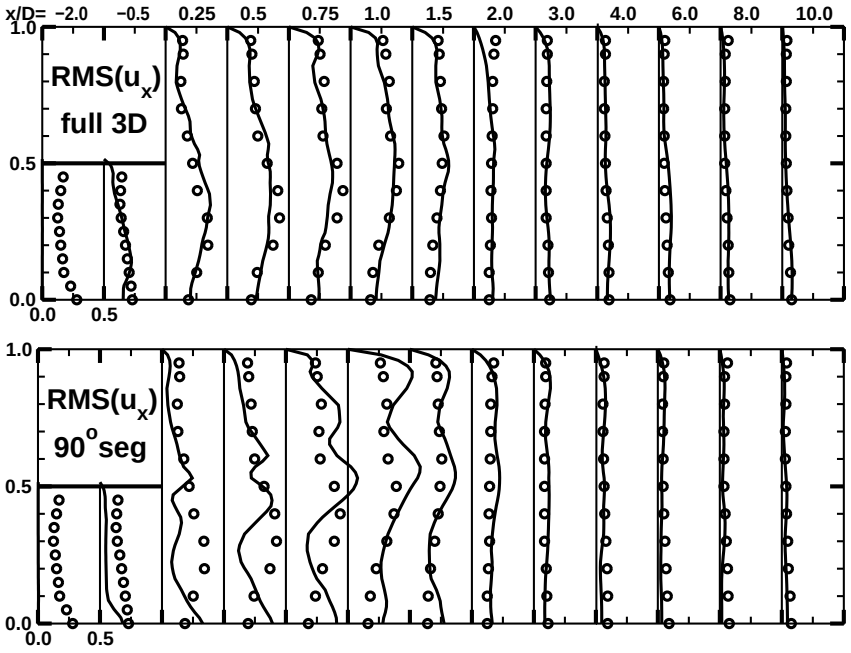

Figure 14: Expansion flow, S=0.6, $\overline{u_x'^2}$ axial turbulence intensity, solid lines: LES computation, circles: experimental data, above: 3D full, below: 3D 90° axi-symmetric, averaging time-span: 0.2s

the swirl flow to create turbulence and enhance mixing. The high production rate of turbulence of the recirculation zone is one of the reasons for the good ignition characteristics of swirl burners.

The same observations made for the axial velocity $\overline{u}_x$ apply to the azimuthal velocity component $\overline{u}_\phi$ of the swirl flow (fig. 15). The mean values of the full 3D computation are in excellent agreement with the experiment. The axi-symmetric computations overpredict the azimuthal momentum close to the axis. Again, this can be explained by the missing radial turbulent transport.

A look at the azimuthal turbulence intensity $\overline{u_\phi'^2}$ reveals some interesting observations (fig. 16). Again, the full 3D computation is in good agreement. Note, that the azimuthal turbulence intensity is not zero on the axis. Since in the axi-symmetric computations $u_\phi = 0$ is imposed on the axis at every instant, u_ϕ' has to be zero as well. The comparison of the axi-symmetric computations with the experiment show the greatest deviation on the axis. Because the inner recirculation zone is bound to the axis and can not move crosswise to the flow, the azimuthal turbulent intensities are underestimated throughout the domain.

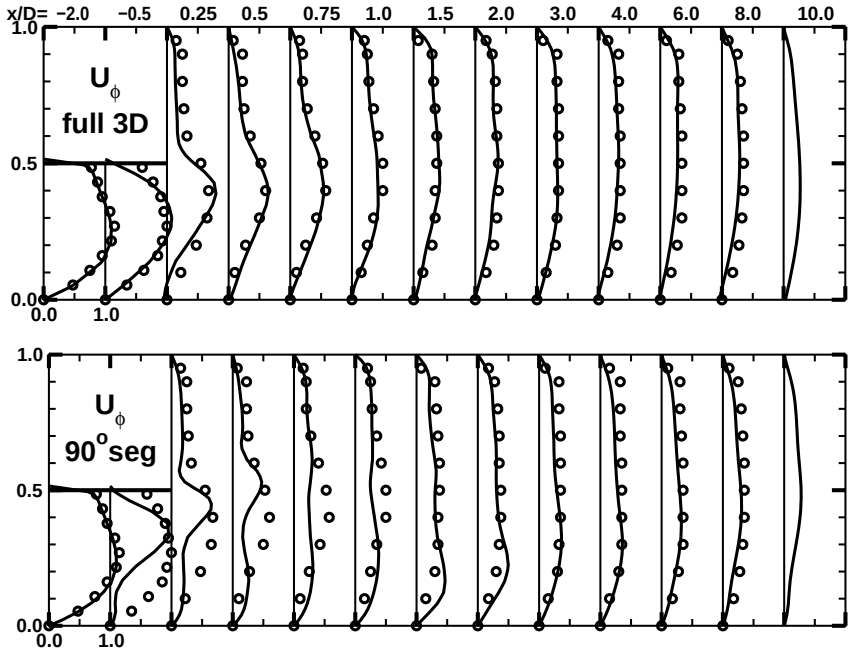

Figure 15: Expansion flow, S=0.6, $\overline{u}_\phi$ azimuthal component, solid lines: LES computation, circles: experimental data, above: 3D full, below: 3D 90° axi-symmetric, averaging time-span: 0.2s

4.4 Computing Efforts

The motivation for the axi-symmetric simplification was to reduce the computational costs. The computational effords of the axisymmetric computation was lower by a factor of 3.24 compared to the full 3D computation.

The computational costs do not depend linearly with the number of mesh points. In the present implementation, the periodic patches in the axi-symmetric cases need a special treatment in the flow solver. This exchange of information between the two periodic patches causes additional communication between processors, which slows down the axisymmetric computation.

5 Conclusions

In order to assess the applicability of the axisymmetric approach to LES computations, two different grid topologies were investigated to reproduce an expansion flow and a swirl flow with LES: a full 3D and a 3D 90° axi-symmetric geometry.

The LES approach has shown, that it can reproduce expansion flows and swirl flows, if the full 3D mesh is used. Already with a low number of mesh

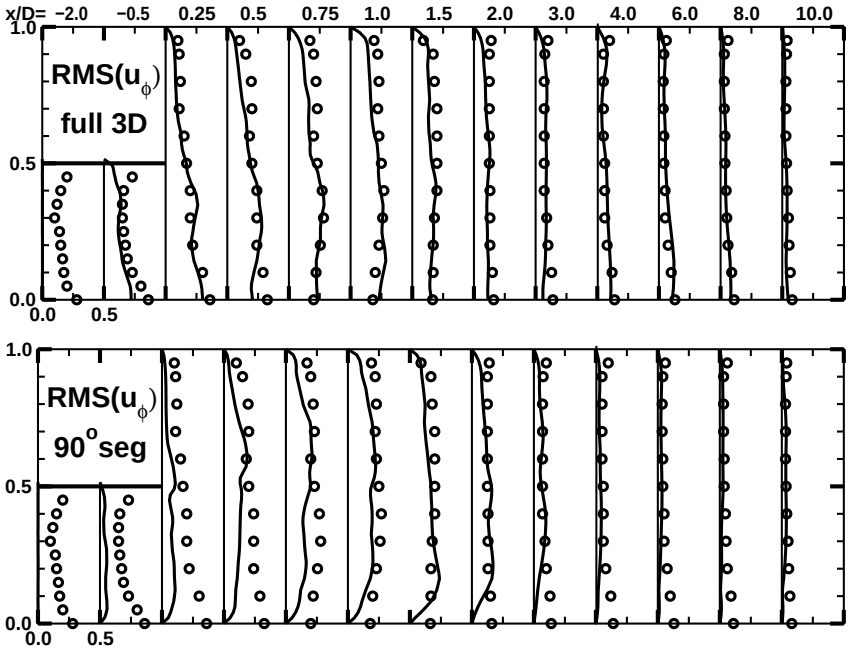

Figure 16: Expansion flow, S=0.6, $\overline{u_\phi'^2}$ azimuthal turbulence intensity, solid lines: LES computation, circles: experimental data, above: 3D full, below: 3D 90° axi-symmetric, averaging time-span: 0.2s

points it is possible to obtain reasonably good results. This can be explained with the fact, that the here computed flows are dominated and characterized by large scale turbulence, which is resolved even on coarse meshes.

The impact of the axisymmetric approach on LES was discussed. The error in the LES computations using an axisymmetric assumption were high. Especially in the computations of the swirl flow the axisymmetric computations did not even reproduced the basic flow characteristics properly. The unexpected high error induced by the axisymmetric assumption make the usage of this approach little advisable. Although the gain in computational costs was remarkably, in the author's opinion they do not justify the usage of an axisymmetric approach for these kind of flows. However, since the failure of the axisymmetric assumption for LES can be associated with the underprediction of the radial turbulence intensity on the axis, the 3D axisymmetric approach might still have an area of application on flows where naturally no turbulence is present on the axis (e.g. an axisymmetric diffuser) or the axis of symmetry is not part of the flow (e.g. a blade of a turbo fan).

The full 3D LES computations have shown, that they can predict flows of interest for industrial applications. Despite the high costs of the 3D LES, the advantages of this approach are promising in order to predict practical flow

configurations.

6 Acknowledgements

This work has been carried out with the support of the gas turbine department of Siemens Power Generation KWU.

References

[Akselvoll and Moin, 1996] Akselvoll, K. and Moin, P. (1996). Large-eddy simulation of turbulent confined coannular jets. *Journal of Fluid Mechanics*, 315:387–411.

[Colin et al., 2000] Colin, O., Ducros, F., Veynante, D., and Poinsot, T. (2000). A thickened flame model for large eddy simulations of turbulent premixed combustion. *Phys. Fluids*, 12(7):1843–1863.

[Dellenback, 1986] Dellenback, P. A. (1986). *Heat transfer and velocity measurements in turbulent swirling flows through an aprupt axisymmetric expansion.* PhD thesis, Arizona State University.

[Dellenback et al., 1988] Dellenback, P. A., Metzger, D. E., and Neitzel, G. P. (1988). Measurements in turbulent swirling flow through an aprupt axisymmetric expansion. *AIAA Journal*, 26(6):669–681.

[Ducros et al., 1997] Ducros, F., Nicoud, F., and Schönfeld, T. (1997). Large eddy simulation of compressible flows on hybrid meshes. In *11th Symposion on Turbulent Shear Flows*, volume 3, pages 28–1 – 28–6.

[Escudier and Zehnder, 1982] Escudier, M. P. and Zehnder, N. (1982). Vortex flow regimes. *Journal of Fluid Mechanics*, 115:105–121.

[Faler and Leibovich, 1977] Faler, J. H. and Leibovich, S. (1977). Disrupted states of vortex flow and vortex breakdown. *Phys. Fluids*, 20(9):1385–1400.

[Faler and Leibovich, 1978] Faler, J. H. and Leibovich, S. (1978). An experimental map of the internal structure of a vortex breakdown. *Journal of Fluid Mechanics*, 86:313–335.

[Farokhi et al., 1989] Farokhi, S., Taghavi, R., and Rice, E. J. (1989). Effect of initial swirl distribution on the evolution of a turbulent jet. *AIAA Journal*, 27(6):700–706.

[Guo et al., 2001] Guo, B., Lnangrish, T., and Fletcher, D. (2001). Simulation of turbulent swirl flow in an axisymmetric sudden expansion. *AIAA Journal*, 41(1):96–102.

[Gupta et al., 1984] Gupta, A. K., Lilley, D. G., and Syred, N. (1984). *Swirl Flows*. Energy and Engineering Science. Abacus Press.

[Hogg and Leschziner, 1989] Hogg, S. and Leschziner, M. A. (1989). Computation of highly swirling confined flow with a Reynolds-stress turbulence model. *AIAA Journal*, 27(1):57–63.

[Krebs et al., 1999] Krebs, W., Walz, G., Hoffmann, S., and Judith, H. (1999). Detailed thermal analysis of annular combustors. *ASME*, (99-GT-45).

[Pierce and Moin, 1998a] Pierce, C. and Moin, P. (1998a). Large eddy simulation of a confined coaxial jet with swirl and heat release. *AIAA Paper*, (AIAA 98-2892).

[Pierce and Moin, 1998b] Pierce, C. D. and Moin, P. (1998b). Method for generating equilibrium swirling inflow conditions. *AIAA Journal*, 36(7):1325–1327.

[Poinsot and Lele, 1992] Poinsot, T. J. and Lele, S. K. (1992). boundary conditions for direct simulations of compressible viscous reacting flows. *Journal of Computational Physics*, (101):104–129.

[Rodi, 1996] Rodi, W. (1996). *Large-eddy simulations and statistical turbulence models: complementary approaches*, volume New Tools in Turbulence Modelling of *Les edition physique*, chapter 3, page 48ff. Springer.

[Schlüter et al., 2001] Schlüter, J., Schönfeld, T., Poinsot, T., Krebs, W., and Hoffmann, S. (2001). Characterization of confined swirl flows using large eddy simulations. *ASME TURBO EXPO 2001*, (2001-GT-0060).

[Schlüter, 2000] Schlüter, J. U. (2000). *Large Eddy Simulations of Flow and Mixing in Jets and Swirl Flows: Application to Gas Turbines*. PhD thesis, CERFACS, Toulouse, France.

[Schönfeld and Rudgyard, 1998] Schönfeld, T. and Rudgyard, M. (1998). COUPL and its use within hybrid mesh CFD applications. In Ecer, A., Emerson, D., Periaux, J., and Satofuka, N., editors, *Proceedings of the 10th International Conference on Parallel CFD 9 8*, pages 433–440, Hsinchu, Taiwan. Elsevier Science Publishers.

[Schönfeld and Rudgyard, 1999] Schönfeld, T. and Rudgyard, M. A. (1999). Steady and unsteady flows simulations using the hybrid flow solver AVBP. *AIAA Journal*, 37(11):1378–1385.

[Smagorinsky, 1963] Smagorinsky, J. (1963). General circulation experiments with the primitive equations, I, the basic experiment. *Mon. Weather Rev.*, 91(3):99–152.